Evaluating Performance of Heating, Ventilation & Air Conditioning Duct Communication Channel at 60 GHz Using Ray Tracing

Esha Bangar* **and Kamran Kiasaleh**

Abstract—In this paper, we developed a 3-dimensional (3D) ray-tracing simulator using MATLAB for establishing the viability of heating, ventilation, and air conditioning (HVAC) ducts as a reliable communication channel for indoor communication at millimeter-wave (mm-wave) frequencies. We present theoretical analysis of image theory ray-tracing and provide the equations for total electric field due to different rays undergoing reflections at the duct walls. We also computed the received signal strength indicator (RSSI) for the dry and moisture-laden air flowing through the HVAC ducts. The ray-tracing results are compared with the experimental and theoretical results we obtained for the HVAC ducts. With transmitter effective isotropic radiated power (EIRP) of 7 dBm, we obtain RSSI which varies between -34 dBm and -53 dBm for dry atmospheric pressure and temperature of 1013.25 hPa and 294.26 K, respectively, and duct lengths of up to 8 m at 60 GHz.

1. INTRODUCTION

The demand for high data rates has increased exponentially due to the rapid growth in technology, which justifies an increased interest in the millimeter-wave (mm-wave) bands, including 60 GHz band. However, there are several issues, which should be addressed to make the optimum use of the available bandwidth in the mm-wave channels. A key concern is that the signals at higher frequencies suffer from greater propagation losses, and, in general, are severely attenuated by physical barriers, such as walls, doors, etc. in the indoor environment. Therefore, these barriers limit signal transmission to line-of-sight (LOS) communication scenario, such as the one encountered in an indoor communication within a room in the house.

In [1], we introduced the concept of HVAC ducts that can be used as a potential communication channel. HVAC ducts are hollow cylindrical or square metal pipes that act as large waveguides through which the mm-wave signal can travel without suffering much attenuation from the physical barriers or time-varying factors, such as the movement of people, leading to many folds increase in the coverage area and providing a non-LOS communication throughout a house or a building. We also calculated the total number of modes present in straight HVAC ducts and the power associated with these modes [1]. We presented the theoretical channel frequency response as well. This paper also shows the experimental results, such as signal to noise ratio (SNR), error vector magnitude (EVM), and bit error rate (BER), which justify the use of HVAC duct as a viable communication medium. In [2], we investigated physical channel parameters, such as power delay profile and root-mean-square (RMS) delay spread related to a straight as well as other shapes of an HVAC duct. In this work, we calculated and measured the mm-wave HVAC duct channel frequency responses and its time counterpart, the impulse response, for the different shapes of HVAC ducts. We also calculated the theoretical received signal strength indicator (RSSI) for the HVAC duct of different bend angles and studied various dispersions (intramodal, intermodal, and multipath dispersion) that occur inside the duct. To further gain insight, we compared the theoretical

RSSI level to those obtained through experiments performed using Tensorcom chipsets with different shapes and lengths of HVAC ducts.

Authors in [3] present a comprehensive review on ray-tracing (RT) techniques, focusing on the fundamental concepts and practical ray tracing algorithms. The paper describes the ray concept, ray propagation phenomenon such as line-of-sight, reflection, transmission, diffusion, and scattering. Different ray-tracing algorithms, such as Fermat's principle, image-method, shooting and bouncing rays, and hybrid methods are discussed as part of this review paper. Authors also present the different categories of accelerator algorithms for the ray-tracing, such as space-division, 2-dimensional simplification, and graphic process unit (GPU) acceleration. In [4], researchers used RT simulation to find the channel properties for indoor communications. Authors used the results of RT to define a deterministic channel impulse response. The authors in [5] defined the channel propagation for a tunnel using an RT algorithm and calculated the path-loss (PL) for different shapes of tunnels based on the ray-tracing technique. Due to the similarities in the tunnel and the HVAC duct environment, the results of this paper are used here to analyze an HVAC channel. Channel propagation for a tunnel was also explored by authors in [6] using the Shooting and Bouncing Ray (SBR) algorithm and calculations for electromagnetic loss based on the Fresnel's law and UTD (Uniform Theory of Diffraction) were also performed. The authors described a novel 3D simulator called RayLA using JAVA library and Java open graphics library (JOGL) for the SBR algorithm. The study compares the experimental results to the ray-tracing simulations performed for the tunnel at 2.4 GHz.

The study in [7] evaluated the performance of beamforming techniques in multi-user indoor environment at the mm-wave frequency band using both measurements and RT simulations. Channel impulse response was measured, and subsequently power level for the received signals was calculated for different locations of the receiver in a 21 m × 21 m room. Based on these measurement results, various beam forming schemes were adopted, resulting in a beam search algorithm. Further, results of the experiment were compared to the results of a custom 3D ray-tracing simulator. Authors proved that ray-tracing is a reliable directional channel model for beamforming assessment and for real-time assistance in the beam-searching phase.

The paper in [8] investigated the system level performance of mm-wave 60 GHz channels by simulating a realistic living room scenario considering the effects of human shadowing and three different types of antennas. Authors measured the channel impulse response (CIR) using a 3-dimensional (3D) RT method. The results were then fed to a channel simulator to generate the performance figures. Authors showed that it becomes eminently challenging to maintain the communication link due to the obstruction of the LOS or due to the presence of multiple strong reflection paths using an omnidirectional antenna. It was suggested to incorporate directional antenna with high gain capable of performing beamforming for the 60 GHz indoor communication systems. In [9], a millimeter-wave quasi-deterministic (Q-D) channel model for an in-room access scenarios were developed with double-directional channel measurements using a custom developed channel sounder at 58.5 GHz. From the measured data, the multi-path components were extracted, and an intra-cluster model was developed based on the actual physical propagation paths to identify the scattering processes explicitly on the rough surfaces. Ray-tracing simulations were performed and compared to the experimental results and authors found them to be similar.

Several other authors [10–20] performed extensive channel sounding experiments for millimeter wave channels in case of indoor communication environments, calculated the channel impulse response, and characterized the path loss for the different transmitter and receiver separations, human blockage, obstructions in the form of walls, cabinets, and furniture. Authors in [11] also considered polarimetric diffuse scattering channel model and recorded the channel measurements at 26 GHz and 60 GHz. As the indoor environment can have several rough surfaces and edges, and when the signal impinges on these surfaces scattering will take place, the authors explored the polarimetric diffuse scattering channel measurements. Phased arrays were utilized by the authors in [12] to estimate the ray paths with the knowledge of beam patterns of the phased arrays. Authors also performed ray-tracing simulation to verify the results at mm-wave frequencies.

Since experimental measurements are not always feasible due to the high cost of mm-wave transceivers, authors in [21–37] have also described various ray-tracing simulations based on SBR/IM. Ref. [21] presents the propagation characteristics of mm-wave signals in the indoor radio channel based

on the method of shooting and bouncing ray tracing/image method and analyzed the path-loss models, received power and the root-mean-square delay spread. The paper also considers the line-of-sight and non-line-of-sight (NLOS) scenarios and observes a path-loss exponent of 3.87 for NLOS scenario. Authors in [22] performed a research on the transmission coverage area using ray-tracing simulations for a train compartment and an indoor conference room. The transmitter was mounted on the ceiling and the maximum transmitter-receiver separation distance considered was 8 m for which the received signal is recorded to be -100 dBm.

To validate the viability of an HVAC duct as a communication channel, a precise study of the radio propagation channel should be performed. One way to evaluate the HVAC duct channel characteristic is to measure the CIR for various duct shapes and lengths. However, the ability to obtain the CIR is limited because these measurements will be specific to the duct structure. Also, measurements can be expensive in the mm-wave band as compared to the electromagnetic simulation approaches, such as RT. RT simulations are widely adopted to estimate radio channels for tunnels, trains, and other indoor environments, alleviating the burden of extensive field measurements. By implementing a reliable 3DRT approach, many useful physical parameters can be extracted. Also, the additional information such as the angle of arrival, angle of departure, complex amplitude and delay of each multipath component can be obtained by RT while acquiring such parameters through experimental measurements are generally tedious. Moreover, the impact of antenna pattern and mutual coupling can be easily included in the RT simulation. These capabilities make the RT approach a powerful tool to predict channel path-loss and to calculate parameters such as SNR, EVM, and BER. Two major methods of implementing 3D RT are image theory and SBR. For uniform structures such as HVAC ducts, RT via image theory will be easier to implement, and will lead to a reduction in the simulation time. For a symmetrical structure, image method is best suited as it can be easily extended to accommodate multiple reflections. The procedure involves calculation of the image of the transmitter and the receiver from all the reflecting surfaces, therefore, is recursive and can be easily implemented as a computer algorithm. SBR method attempts to trace every ray path from the origin to the reception, considering a ray-tube structure for each ray launched. It involves assumption of a sphere which can be divided into equal number of symmetric surfaces which are considered as the ray-fronts. The method can consume more time depending on the complexity of the geometry, further total number of rays received can be misrepresented. Accelerator methods, which can significantly reduce the time required for the simulation, can be implemented for both image method and SBR, which involve space division, 2-dimensional simplification and GPU acceleration.

In this study, we developed an RT simulator based on image theory using MATLAB to study the mm-wave HVAC duct communication channel. Our simulator incorporates antenna beamwidth to estimate the accurate number of rays being launched. We also include an attenuation component to represent atmospheric losses due to the temperature and moisture present in the air flowing through the HVAC ducts. The consideration of the printed half-wave dipole antenna is motivated by the fact that such antennas provide large gain over a wide bandwidth and lend themselves to easy system integration. The simulation accuracy is verified with the comparison between simulated and measured experiment data using the Tensorcom WiGig compliant chipsets. The simulator is designed to specifically work only for mm-wave frequencies and for symmetrical structures to reduce the simulation time considerably.

2. RAY-TRACING USING IMAGE METHOD

The RT method adopted in this paper is based on the ray optics which aims at solving Maxwell's equations with the assumption of operation limited to the mm-wave frequency band. This assumption has a crucial effect due to the large dimension of the HVAC duct compared to the wavelength of the mm-wave band. The RT image theory method uses less computer memory due to the symmetrical structure of the HVAC duct. We note that the number of incident rays and the angle of incidence depend on the beamwidth of the printed dipole antenna. We consider the transmitter with a printed half-wave dipole antenna with a beamwidth of $\pm 30°$.

The trajectory of the reflected rays is determined through the image method and Fermat's principle of the least time. The Fermat's principle states that a ray will travel from the transmitter to the receiver through a path, which will require the least possible time. Further using image method, we consider that

a ray launched by the transmitter T_x will reach the receiver R_x after reflection from the duct boundary if the image of the transmitter T_x^i (superscript "i" represents the transmitter image outside the HVAC duct) can be connected to the receiver through a straight line, as shown in Fig. 1. In this case, the image T_x^i is considered as a new transmitter. The same process can be applied to find the ray path with multiple reflections. The recursive procedure is implemented efficiently using MATLAB. All the rays launched by the transmitter will always reach the receiver due to the symmetrical structure of the HVAC duct. However, the rays will have different path lengths, phase angles, and delays. Moreover, the electric field strength is reduced due to the reflection from the HVAC duct walls as the ray progresses. Therefore, the magnitude of the reflected field is determined by Fresnel's equation whereas the propagation direction is determined by the law of reflection. Unlike theoretical and empirical models, the RT method does not provide simple formulas for the calculation of path loss. Hence, one has to resort to theoretical calculation of path loss based on the value of the average pointing vector obtained from ray-tracing simulation and the effective area of the transmitting and receiving antenna.
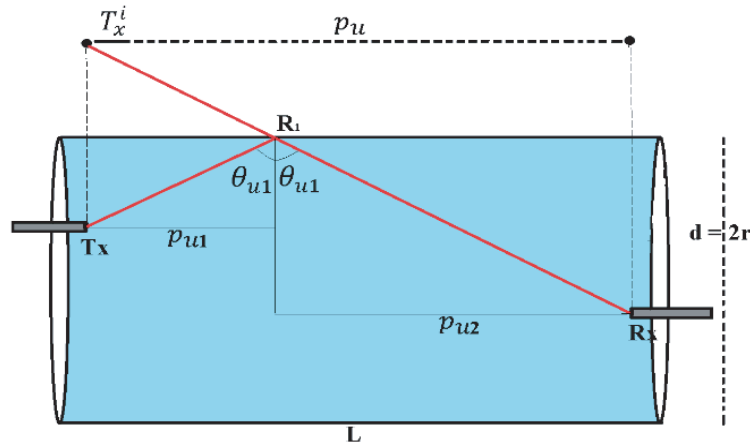
Figure 1. Ray tracing with image method for HVAC duct.

3. IMPLEMENTATION OF RAY-TRACING ALGORITHM

We consider an HVAC duct of diameter d (radius $r = d/2$) and the length L for the implementation of ray tracing. Let the coordinates of T_x and R_x be $(x_T,\ y_T,\ z_T)$ and $(x_R,\ y_R,\ z_R)$, respectively. The projection of the direct path from the transmitter to the receiver on the upper duct wall is represented by p_u and on the lower duct wall is represented by p_l. In the case of a straight HVAC duct, $p_u = p_l$. Consider a ray which has one reflection point R_1 between the transmitter T_x and the receiver R_x. The distance between the transmitter image T_x^i and R_1 is assumed to be p_{u1}, and the distance between R_1 and the receiver R_x is assumed to be p_{u2}. Therefore, $p_u = p_{u1} + p_{u2}$. The incident angle which the ray makes with the upper duct wall is given as

$$\theta_{u1} = \arctan\left(\frac{p_{u1}}{d - z_T}\right) \tag{1}$$

The reflected angle which the ray makes with the upper duct wall is given as

$$\theta_{u1} = \arctan\left(\frac{p_{u2}}{d - z_R}\right) \tag{2}$$

From Eqs. (1) and (2), we get,

$$\tan\left(\theta_{u1}\right) = \frac{p_u}{2d - z_T - z_R} \tag{3}$$

The circular dimension of the HVAC duct will be very small compared to the length of the duct. However, the wavelength of the mm-wave is even smaller than the circular dimension of the HVAC

duct. Therefore, the difference between the height of the transmitter and the receiver inside the duct will be fairly small, i.e., $z_T - z_R = \delta$ can be ignored. Therefore,

$$\tan(\theta_{u1}) \approx \frac{p_u}{2d - 2z_T} \tag{4}$$

If a ray is reflected twice, once from the upper wall at R_1 and then from the lower wall at R_2, then p_u can be divided into three parts as $p_u = p_{u1} + p_{um} + p_{u2}$ (following the same approach as one reflection case, see Fig. 2).
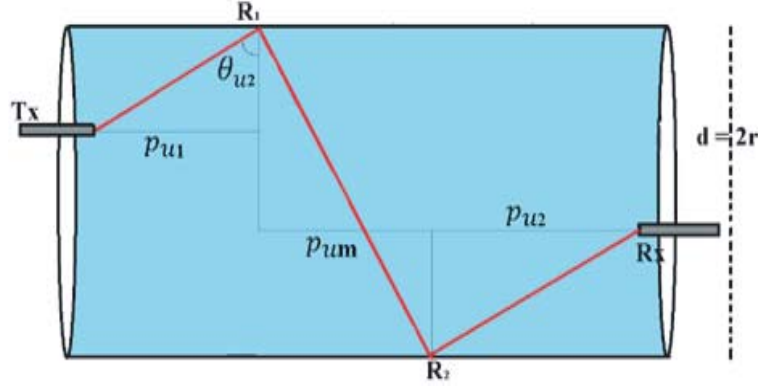
Figure 2. Ray tracing with two reflections inside the HVAC duct.

If a ray is reflected twice, once from the upper wall R_1 and then from the lower wall R_2, then p_u can be divided into three parts as $p_u = p_{u1} + p_{um} + p_{u2}$ (following the same approach as one reflection case, see Fig. 2). The angle which the transmitted wave makes with the normal to the upper duct wall is represented as θ_{u2}. Further this angle will be the same as the angle which the reflected wave will make with the normal to the lower duct wall and so on. Therefore, for the distance between the transmitter T_x and reflection point R_1 the tangent of the angle θ_{u2} can be represented as

$$\tan(\theta_{u2}) = \frac{p_{u1}}{d - z_T} \tag{5}$$

For the last part of the distance between the reflection point R_2 and receiver R_x, the angle θ_{u2} can be represented as

$$\tan(\theta_{u2}) = \frac{p_{u2}}{z_R} \tag{6}$$

For the distance p_{um} the angle can be written as

$$p_{um} = \tan(\theta_{u2})[d - z_R + z_R] = d\tan(\theta_{u2}) \tag{7}$$

From Eqs. (5), (6), and (7), we get,

$$\tan(\theta_{u2}) = \frac{p_u}{2d - z_T + z_R} \approx \frac{p_u}{2d} \tag{8}$$

The last part of Eq. (8) is calculated using $z_T - z_R = \delta \ll d$. Following the above approach, we calculate the incident angle for a ray that gets reflected n times. We consider that an upward-directed ray makes an angle θ_{un} and a downward-directed ray makes an angle θ_{ln} at each reflection point. Then, the tangent of these angles is given, respectively, as (see Appendix A)

$$\tan(\theta_{un}) = \frac{p_u}{r[1 + 2n - (-1)^n] + z[(-1)^n - 1]} \tag{9}$$

$$\tan(\theta_{ln}) = \frac{p_l}{r[-1 + 2n + (-1)^n] + z[(-1)^{n+1} + 1]} \tag{10}$$

The distance of the nth order reflection point from the transmitter is given by the denominator of Eq. (10). Similar calculations have been done earlier in case of the tunnels, but there are several

differences between these two studies. The frequency considered in [5] is 1 MHz which presents a completely different situation than the frequencies in the mm-wave band. Secondly, the materials used in the construction of the tunnel have a relative permittivity which is not encountered in the case of HVAC duct as these are made up of galvanized steel in general. Thirdly, the distance between the transmitter and the receiver considered in the case of tunnels is in kilometers, whereas the work in this paper is particularly targeting indoor communication restricting the distance to a few meters. Lastly, HVAC ducts will always have smooth wall surface and symmetric shapes compared to the tunnels, which justifies the use of geometric optics to calculate the angles made by the different incident rays. Note — due to the smooth and polished interior surface of the HVAC duct, the propagation-mechanism scattering will be limited and therefore, is not considered as a crucial hindrance in this study.

Another important parameter is the loss in the electric field energy due to the reflection at the duct walls. In general, Fresnel law defines the reduction in the EM wave's energy after every reflection in terms of the Fresnel reflection coefficients. However, since the HVAC ducts are made using galvanized steel, the reflection coefficient is simplified to -1. Consider a total of M rays with each ray getting reflected N times. The θ component of the radiated electric field amplitude in the spherical coordinate system from a half-wave dipole antenna can be written as

$$E_\theta\left(r,\theta\right)=\frac{j\eta I}{2\pi r}\frac{\cos\left(\dfrac{kl}{2}\cos\left(\theta\right)\right)}{\sin\left(\theta\right)}e^{-jkr} \tag{11}$$

where I is the input current in the antenna; $\eta=\sqrt{\mu_0/\epsilon_0}$ is the intrinsic impedance of the vacuum with μ_0 and ϵ_0 denoting the permeability and permittivity of free space, respectively; $k=2\pi/\lambda$ is the wavenumber; l is the length of the antenna, which is approximately $\lambda/2$ for a half-wave dipole; and r is the distance between the transmitter and the point of observation in the farfield zone. r will be very small (4 cm) and close to the transmitting antenna because of the antenna size and the frequency of operation. For a half-wave dipole, the electric field in the r and ϕ directions in the spherical coordinate system are zero. Hence, we focus on the electric-field in the θ direction. The electric field will be the same at every point at a distance r and at an angle θ from the antenna. The radiation intensity $U(\theta\phi)$ can be calculated as

$$U\left(\theta,\phi\right)=\frac{r^2}{2\eta}\left|E_\theta\left(r,\theta\right)\right|^2=\frac{\eta I^2}{8\pi^2}\frac{\cos^2\left(\dfrac{\pi}{2}\cos\left(\theta\right)\right)}{\sin^2\left(\theta\right)}\approx\frac{\eta I^2}{8\pi^2}\sin^3\left(\theta\right) \tag{12}$$

The above approximation is considered for $\theta\in[0,\pi]$, which is the range of interest. The average Poynting vector W_T can be calculated from the radiation intensity as

$$W_T=\frac{U}{r^2}=\frac{1}{2\eta}\left|E_\theta\left(r,\theta\right)\right|^2\approx\frac{\eta I^2}{8\pi^2r^2}\sin^3\left(\theta\right) \tag{13}$$

The total radiated power is $P_T=\int_0^{2\pi}\int_0^\pi r^2W_T\sin(\theta)d\theta d\phi$. Equivalently, we have,

$$P_T=\int_0^{2\pi}\int_0^\pi U\left(\theta,\phi\right)\sin\left(\theta\right)d\theta d\phi=\frac{2.43\eta\left|I\right|^2}{8\pi} \tag{14}$$

From Eqs. (13) and (14), we can see that the directivity of the half-wave dipole antenna is given by $D_T=4\pi\max(U)/P_T=4\pi\eta|I|^2/8\pi^2P_T\approx1.65$. Further, for the transmitting antenna, D_T is also related to the antenna gain G_T and radiation efficiency ς_T as

$$D_T=\frac{G_T}{\varsigma_T} \tag{15}$$

Hence, we have

$$W_T=\frac{P_T\sin^3\left(\theta\right)}{2.435\pi r^2}=\frac{P_{in}\zeta_T\sin^3\left(\theta\right)}{2.435\pi r^2}=\frac{P_{in}G_T}{4\pi r^2} \tag{16}$$

where $\theta=90°$ is assumed due to the antenna's orientation. When the antenna introduces the electric field in the HVAC duct, the field rays either reach the receiver directly or by reflection from the HVAC

duct walls. The number of rays which will contribute to the received electric field depend on the type of the antenna and its beamwidth. For a ray r_d which reaches the receiver directly, the radiated electric field will be given as $E_d(r_d, \theta) = E_\theta e^{-jkL}/L$. The average Poynting vector for this component of the field is,

$$W_d = \frac{1}{2\eta}|E_d|^2 = \frac{1}{2\eta}\left|\frac{E_\theta}{L}e^{-jkL}\right|^2 \tag{17}$$

The distance r_d will be equal to the length of the HVAC duct, i.e., $r_d = L$. For the rays which suffer one reflection before reaching the receiver, the radiated electric field can be given as $E_1(r_1, \theta) = \frac{-E_\theta}{r_1}e^{-jkr_1}$. Hence,

$$W_1 = \frac{1}{2\eta}|E_1|^2 = \frac{1}{2\eta}\left|\frac{E_\theta}{r_1}e^{-jkr_1}\right|^2 \tag{18}$$

In Eq. (9), we substitute $n = 1$ to get the distance r_1 as $r_1 = \sqrt{L^2 + (r[1 + 2 - (-1)] + z[(-1) - 1])^2}$. Similarly, for the mth ray which suffers n reflections, the radiated electric field is given as $E_m(r_n, \theta) = (-1)^n \frac{E_\theta}{r_n}e^{-jkr_n}$. Furthermore,

$$W_m = \frac{1}{2\eta}|E_m|^2 = \frac{1}{2\eta}\left|\frac{E_\theta}{r_n}e^{-jkr_n}\right|^2 \tag{19}$$

where $r_n = \sqrt{L^2 + (r[1 + 2n - (-1)^n] + z[(-1)^n - 1])^2}$. The total electric field received at the receiver from all the M rays can be given as

$$E_r = E_d + \sum_{m=1}^{M}E_m = \frac{E_\theta}{L}e^{-jkL} + \sum_{m=1}^{M}(-1)^m\frac{E_\theta}{r_m}e^{-jkr_m} \tag{20}$$

M is calculated by converting the spherical coordinates to Cartesian coordinates $x = \sin(\phi)$ and $y = \cos(\phi)$ where ϕ is the beamwidth and considering antenna's orientation $\theta = 90°$. For this work, we consider the mesh size in Cartesian coordinates to be 10×10, so maximum number of rays which can be transmitted will be $M = (10 - x) \times (10 - y)$. Consequently, the maximum power P_R received at the receiver is given in terms of the average Poynting vector and the maximum effective area of the receiving antenna $A_{R,e}$ as

$$P_R = \frac{|E_r|^2}{2\eta}A_{R,e} = \frac{E_\theta^2}{2\eta}\left|\frac{e^{-jkL}}{L} + \sum_{m=1}^{M}\frac{e^{-jkr_m}}{r_m}\right|^2 A_{R,e} \tag{21}$$

In general, the different rays arrive at different angles, resulting in the effective receiving area that is depending on the angle of arrival of each multipath. In this paper, however, we consider he maximum possible effective area. As will be shown in the Results section, for the practical parameters, the above approximation yields fairly accurate results. From Eq. (13), we can substitute $W_T = |E_\theta|^2/2\eta$ in Eq. (21), which results in,

$$P_R = W_T\left|\frac{e^{-jkL}}{L} + \sum_{m=1}^{M}\frac{e^{-jkr_m}}{r_m}\right|^2 A_{R,e} = \frac{P_{in}G_T}{4\pi r^2}\left|\frac{e^{-jk(L+r)}}{L} + \sum_{m=1}^{M}\frac{e^{-jk(r_m+r)}}{r_m}\right|^2 A_{R,e} \tag{22}$$

The effective area of the receiving antenna is given as $A_{R,e} = \lambda^2 D_R/4\pi$ where λ is the wavelength, and D_R denotes the directivity of the receiving antenna. For the receiving antenna when radiation efficiency $\varsigma_R \approx 1$ is considered and the receiving antenna has the gain G_R, we have $A_{R,e} = \lambda^2 G_R/4\pi$. Therefore, using the value of $A_{R,e}$ in Eq. (22), the maximum total received power P_R can be written as

$$P_R = \frac{\lambda^2 P_{in}G_T G_R}{16\pi^2}\left|\frac{e^{-jk(L+r)}}{L} + \sum_{m=1}^{M}\frac{e^{-jk(r_m+r)}}{r_m}\right|^2 \tag{23}$$

Moreover, an important factor while the HVAC duct is characterized as a viable communication link is the consideration of the temperature and the density of the moisture vapor present in the air flowing

through the duct. The attenuation due to the atmospheric gases flowing inside the HVAC duct is given by $\phi_g = \phi_d + \phi_m$, where ϕ_d and ϕ_m represent the attenuation caused by the dry air and the moisture vapor, respectively. The attenuation caused by dry air is due to its pressure and atmospheric temperature. For, $57\,\text{GHz} \leq f \leq 63\,\text{GHz}$, this parameter is given by [7]

$$\phi_d = \gamma_{57}\frac{(f-60)\,(f-63)}{18} - 1.66 r_p^2 r_t^{8.5}\,(f-57)\,(f-63) + \gamma_{63}\frac{(f-57)\,(f-60)}{18} \tag{24}$$

where γ_{57} and γ_{63} are zero for $57\,\text{GHz} \leq f \leq 63\,\text{GHz}$. However, for $f \leq 57\,\text{GHz}$,

$$\gamma_{57} = \frac{0.0073 f^2 r_p^2 r_t^3}{f^2 + 0.351 r_p^2 r_t^2} + \frac{0.0075 f^2 r_p^2 r_t^2}{(f-57)^2 + 2.44 r_p^2 r_t^5} \tag{25}$$

while $\gamma_{63} = 0$. For $63\,\text{GHz} \leq f \leq 350\,\text{GHz}$, and $\gamma_{57} = 0$

$$\gamma_{63} = \frac{f^2 r_t^{3.5} r_p^2}{5 \times 10^6} - \frac{r_t^{3.5} f^{3.5} r_p^2}{4.2 \times 10^{15}} + \frac{0.004 f^2 r_t^2 r_p^2}{(f-63)^2 + 1.5 r_p^2 r_t^5} + \frac{0.00028 f^2 r_t^4 r_p^2}{(f-118.75)^2 + 2.84 r_p^2 r_t^2} \tag{26}$$

In the above, f [GHz] is the frequency; $r_p = p/1013$; $r_t = 288/T$; p [hPa] is the dry atmospheric pressure; and T is the atmospheric temperature in Kelvin. The attenuation coefficient of moisture vapor depends on the density of moisture vapor ρ in g/m^3 and is given by [7]

$$\begin{aligned}\phi_m = {}& \frac{r_t^2 r_p f^2 \rho}{3 \times 10^5} + \frac{\rho^2 r_t^8 f^2}{6 \times 10^6} + \frac{r_t r_p f^{2.5} \rho}{1.3 \times 10^7} + \frac{0.0004 r_t r_p f^2 \rho}{(f-22.235)^2 + 9.81 r_p^2 r_t} \\ & + \frac{0.001 r_t^2 r_p f^2 \rho}{(f-183.31)^2 + 11.85 r_p^2 r_t} + \frac{4.01 \times 10^{-4} r_t^2 r_p}{(f-325.153)^2 + 10.44 r_p^2 r_t}\end{aligned} \tag{27}$$

The received power P_R at the receiving antenna incorporating the attenuation due to the temperature, pressure, and the moisture content of the gases flowing through the HVAC duct is given by,

$$P_R = \frac{\lambda^2 P_T G_T G_R}{16\pi^2 \phi_g}\left| \frac{e^{-jk(L+r)}}{L} + \sum_{m=1}^{M}\frac{e^{-jk(r_m+r)}}{r_m} \right|^2 \tag{28}$$

The path loss is defined as $PL\,(\text{dB}) = 10\log_{10}(P_T/P_R)$. The received signal strength indicator (RSSI dBm) takes into account the path loss suffered by the rays while traveling through the HVAC duct and is given as [1]

$$RSSI = EIRP - PL\,(\text{dB}) \tag{29}$$

where $EIRP$ is the effective isotropic radiated power from the transmitter and measured in dBm.

4. RESULTS

We consider a rectangular HVAC duct for the 3D ray-tracing simulation, as the ray-tracing effects for the cylindrical and the rectangular HVAC duct will be similar due to the dimension of the HVAC duct compared to the wavelength of the mm-wave traveling through it. We have assumed that the focus effects/caustics are small with the assumption of the smooth curved surface of the conducting walls of HVAC ducts. The assumption is based on the reasoning that the free-space wavelength of the mm-waves frequency is extremely small compared to the curvature of the HVAC duct. However, in most cases, for cylindrical surfaces caustics will take place and will result in spatial attenuation which is governed by the modified radii of the curvatures of the reflected wavefronts [38]. The dimension of the HVAC duct considered for the simulation is $9\,\text{cm} \times 9\,\text{cm}$. Fig. 3 shows the HVAC duct with the transmitter and the receiver at the two ends of the duct. As the receiver can be placed anywhere in the duct to capture the signa, a section in the center of the HVAC duct is considered as the receive. We can observe the different LOS rays as well as rays experiencing multiple reflections from the duct walls traveling between the transmitter and the receiver. The beamwidth of the transmitter antenna decides the number and the incident angle of the rays.
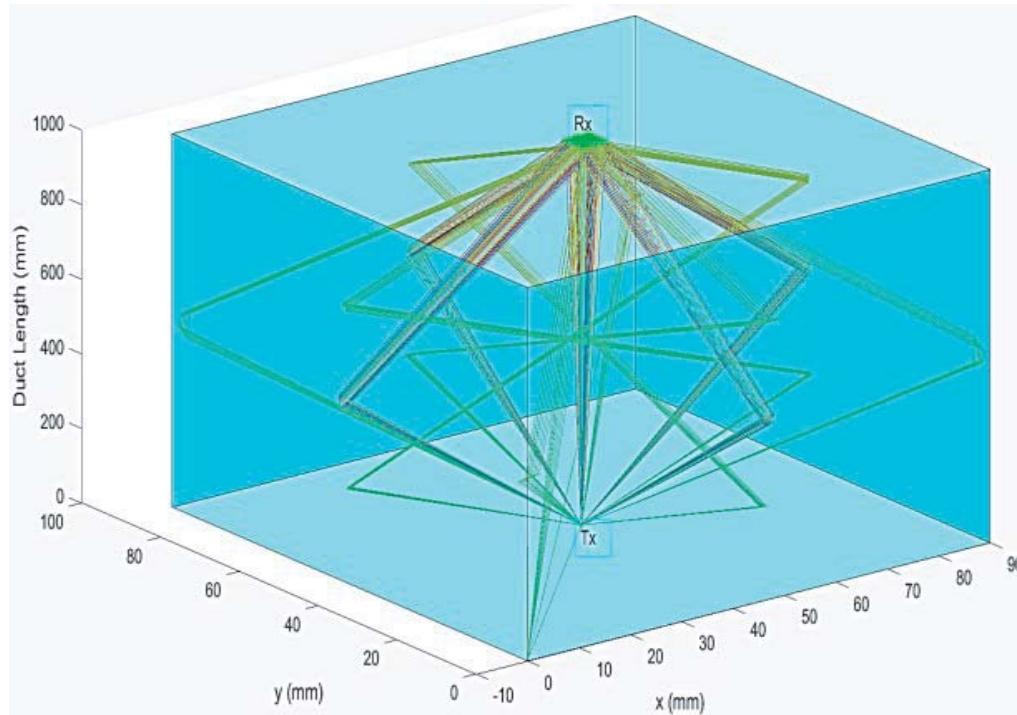
Figure 3. 3D ray tracing inside the HVAC duct with transmitter and receiver at the two ends.

Figure 4 shows the variation of received signal strength indicator (RSSI) for HVAC duct of length 1 m. In Fig. 4, RSSI due to the LOS rays is considered. As the HVAC duct considered for the 3D RT simulation is straight, most of the incident rays reach the receiver without suffering any reflection. The RSSI level for the LOS case is around −23 dBm. Figs. 4(b) and 4(c) show the resulting RSSI due to the rays suffering one and two reflections before reaching the receiver present on the other end of the HVAC duct. The rays are launched at an angle that is confined to ±30° around the transmitter antenna. Therefore, the rays will have different incident angles and will follow the path accordingly. The RSSI level for the one reflection case is around −24 dBm and for the two-reflection case is around −25.5 dBm. We assume that the transmitter effective isotropic radiated power (EIRP) is 7 dBm.

(a)

(b)   (c)
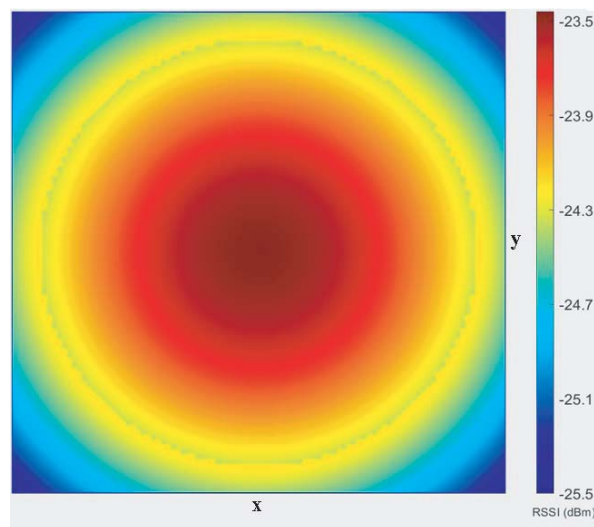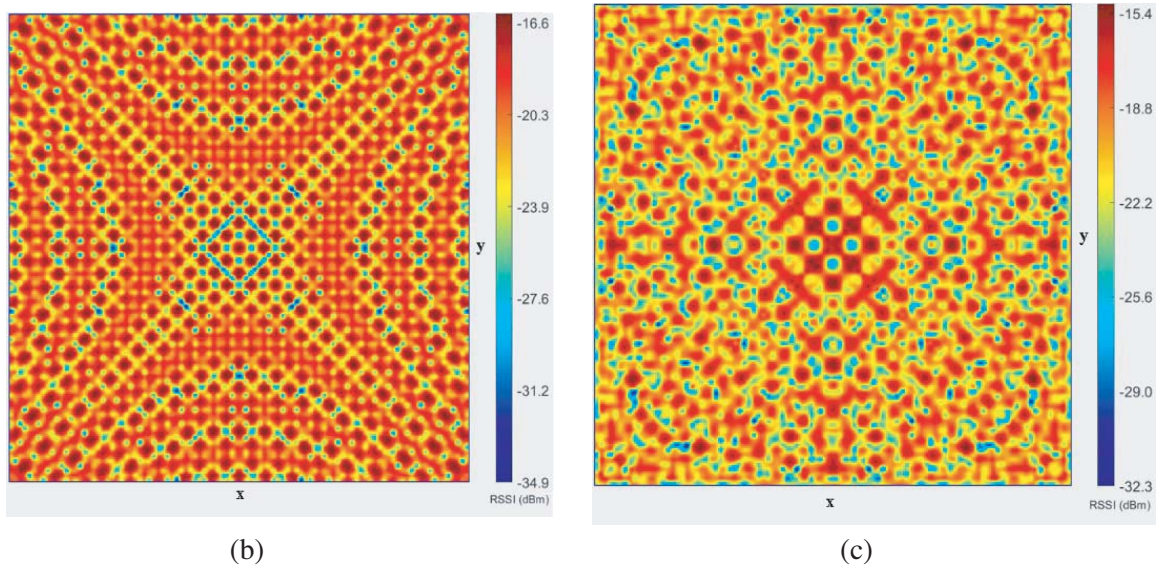
Figure 4. (a) LOS RSSI (dBm) for a HVAC duct length of 1 m. (b) First reflection RSSI (dBm) for a HVAC duct length of 1 m. (c) Second reflection RSSI (dBm) for a HVAC duct length of 1 m.

Figure 5 shows the comparison between the RSSI obtained through the experiment (Exp) and the ray-tracing simulation (RT Sim) as described in this paper. In [1], we performed the experiments with a circular HVAC duct of diameter 12.7 cm and made of galvanized steel. For the experiment we used the Tensorcom chipsets TC60G-USB3-EVB as the transmitter and receiver with the $\pi/2$-BPSK and 1/2 coding rate with a bandwidth of 2.16 GH. The chipsets come with a Linux based speed test application
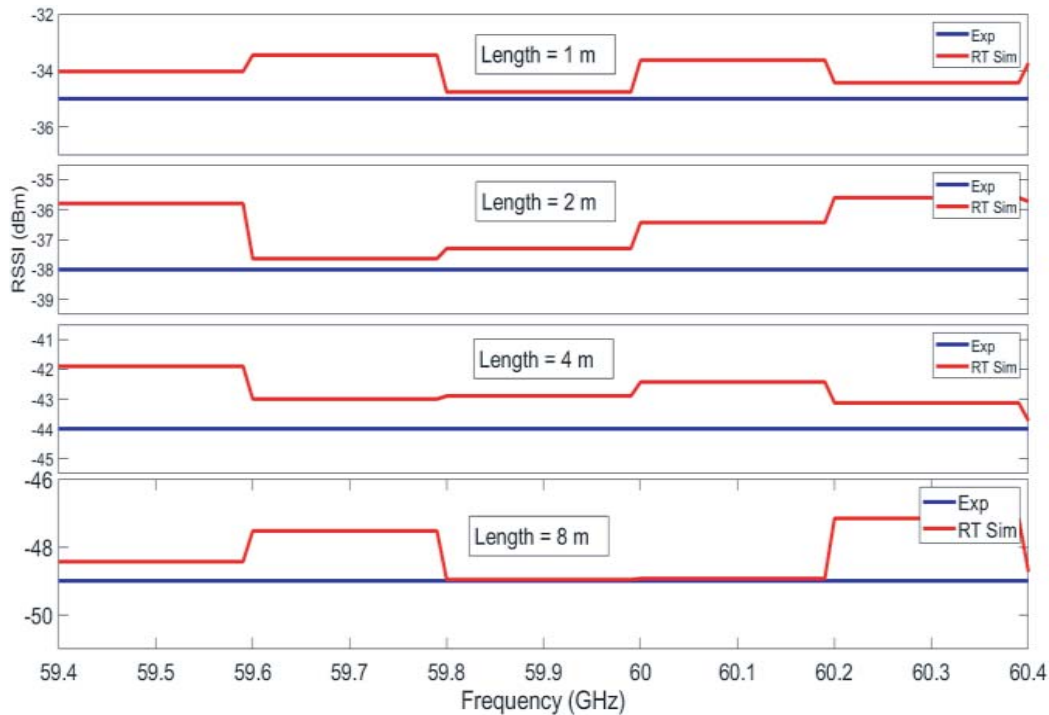
Figure 5. Comparison of RSSI obtained through experimental and ray tracing simulation results for HVAC duct lengths of 1 m, 2 m, 4 m, and 8 m.

(a)

(b)

(c)
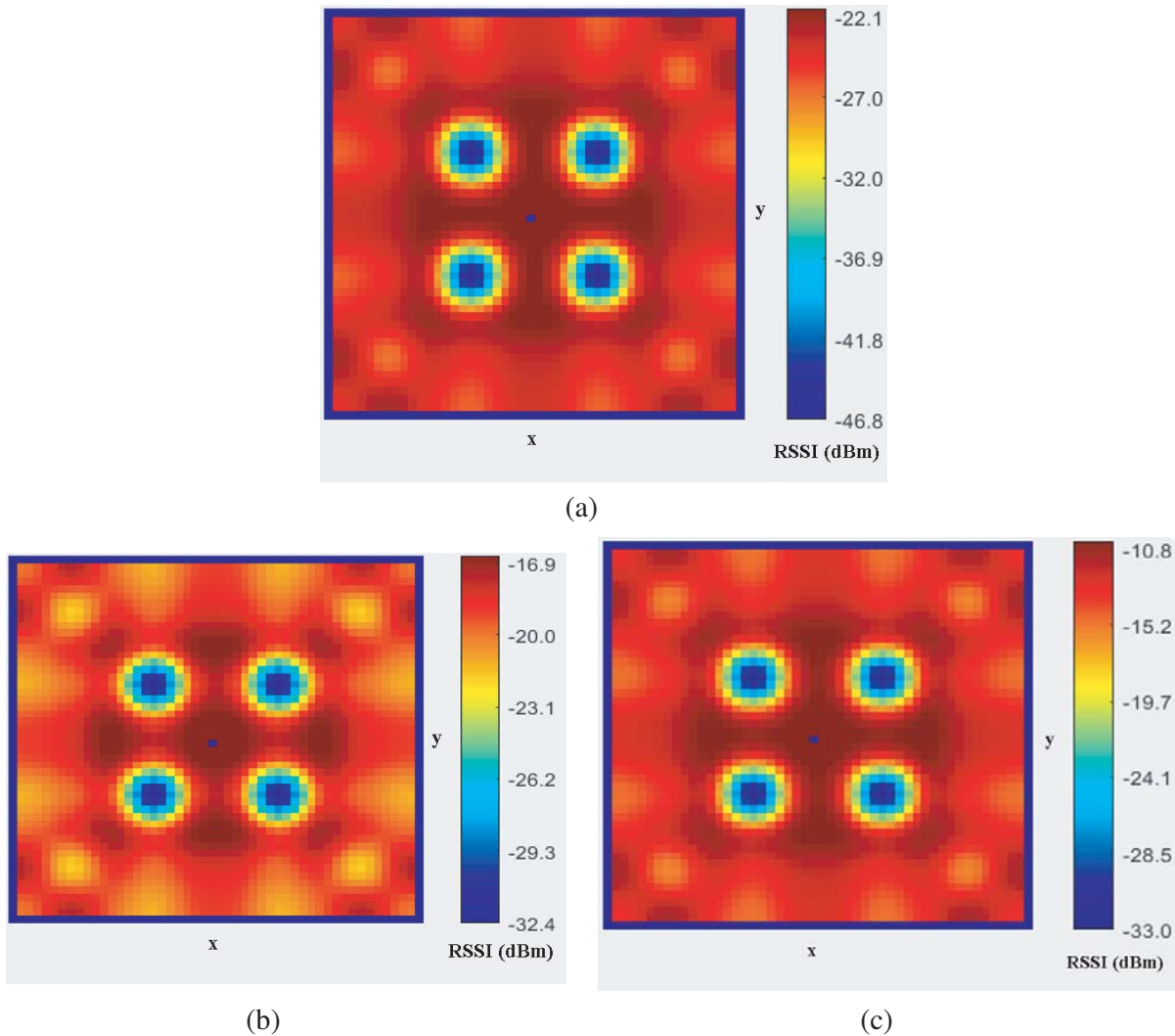
Figure 6. (a) First reflection RSSI (dBm) with antenna beamwidth $\pm 30°$. (b) First reflection RSSI (dBm) with antenna beamwidth $\pm 60°$. (c) First reflection RSSI (dBm) with antenna beamwidth $\pm 90°$.

which we used to evaluate the RF performance of HVAC ducts as well as free space. Using the 3D ray-tracing simulations and calculating RSSI, we have verified the theoretical and experimental results [1, 2]. We obtain RSSI values of -27 dBm, -30 dBm, -35 dBm, and -40 dBm for a straight HVAC duct with the length of 1 m, 2 m, 4 m, and 8 m, respectively. We note that the 3D ray-tracing and the equations presented in the previous section are for the maximum possible received power. Hence, the observed RSSI over the frequency range remains below the simulation results. The difference proves to be only a few dB for most frequencies considered. In general, the results prove the validity and efficacy of the 3D ray-tracing method described in calculating the value of RSSI.

The total number of rays launched in the HVAC duct for the 3D ray-tracing simulation depends on the beamwidth of the antenna used. On varying the antenna beamwidth, the total number of rays launched will vary and will lead to different values of RSSI obtained. However, in most practical antenna designs, the goal is to find a balance between the beamwidth and directivity of the antenna because as the beamwidth increases, the directivity of the antenna decrease. The antenna used in the experimental work [1, 2] has a beamwidth of $\pm 30°$. However, to show the effect of the beamwidth or the total number of rays launched, we compare the RSSI values obtained by ray-tracing simulation for three different beamwidths of $\pm 30°$, $\pm 60°$, and $\pm 90°$ for HVAC duct of length 1 m in Fig. 6. We observe that, in this case, as we consider the broader beamwidth, a larger number of rays reach the receiver, and thereby we

observe an increased RSSI.

The experiment is done using HVAC ducts which are not installed in the buildings, due to which the RSSI results do not account for the temperature and moisture content of the air flowing through the HVAC duct. In Fig. 7, we present a comparison of the experimental RSSI values and the RSSI obtained using Eq. (29) which incorporates temperature and pressure of the air flowing the HVAC duct through the parameter ϕ_g. Air pressure is calculated based on the standards for the air flowing through the HVAC ducts for a given temperature. RSSI values obtained for a temperature range of 288.15 K to 30.15 K are shown in Fig. 7 and compared with the RSSI values obtained using 3D ray tracing simulation without considering any temperature or pressure of the air flowing through the HVAC duct. Further, the results are also compared with the free space path loss (FSPL), which takes place at 60 GHz for different path lengths. We can see from Fig. 7 that the RSSI values for the different values of temperature are almost similar, concluding that the variation in temperature does not have a significant effect on RSSI. However, on comparing the RSSI results obtained by considering the temperature effects to the case when we ignore the effect of temperature and pressure of the air flowing the duct, we observe that the latter is decreased by around 3 dBm for distances up to 4 m and 6 dBm for 8 m. It can also be concluded from Fig. 7 that the RSSI values obtained for the HVAC duct are much higher than those obtained through free space, thereby justifying the use of the HVAC ducts to distribute mm-wave signal.
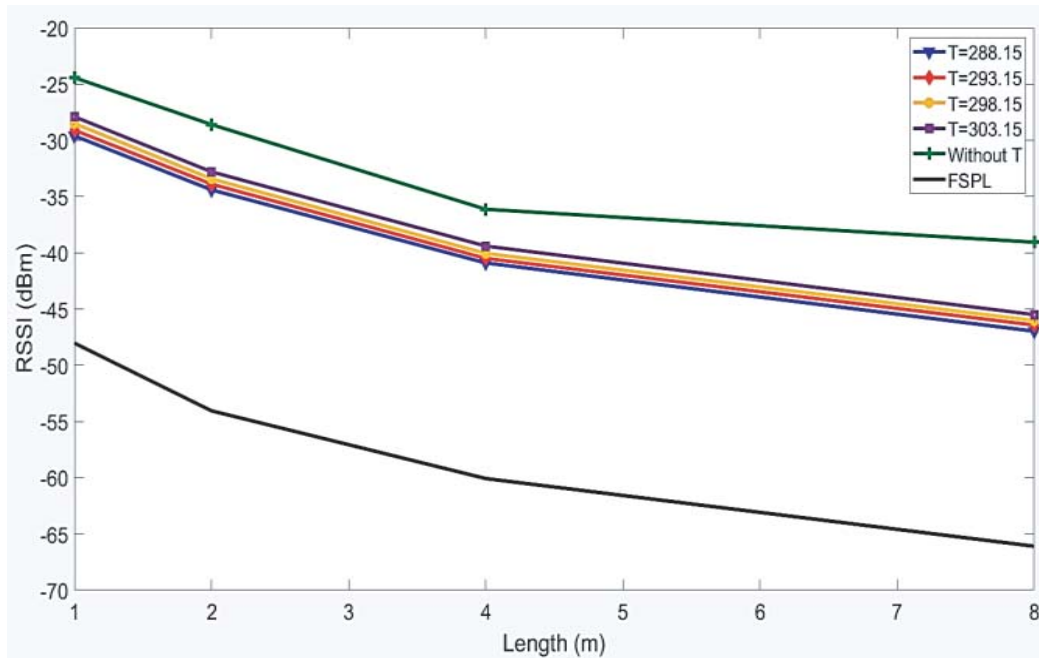
Figure 7. RSSI obtained through RT simulation with and without atmospheric temperature and pressure for HVAC duct. FSPL is shown for comparison.

Figure 8 shows the comparison of the RSSI value obtained using the ray-tracing method described in this paper, while considering the moisture vapor density (g/m^3) of the air flowing through the HVAC duct. The moisture vapor density is varied between $1140 \, g/m^3$ and $1200 \, g/m^3$, and RSSI values are calculated for different duct lengths varying from 1 m to 8 m. Contrary to Fig. 7 where temperature has minimal effect on the RSSI values, moisture vapor density shows significant effect on the values of RSSI obtained for different lengths of HVAC duct. On comparing the RSSI results obtained by considering the moisture vapor density to the case where we ignore the presence of the moisture vapor, we observe that the RSSI is decreased by 11 dBm for distances of up to 4 m and 14 dBm for 8 m in the presence of moisture. However, the results obtained are around 10 dBm above those obtained when considering free space propagation. The point to note in Fig. 8 is that, while we did the theoretical analysis of RSSI values obtained considering the air with moisture vapors present in it, in most practical scenarios, HVAC
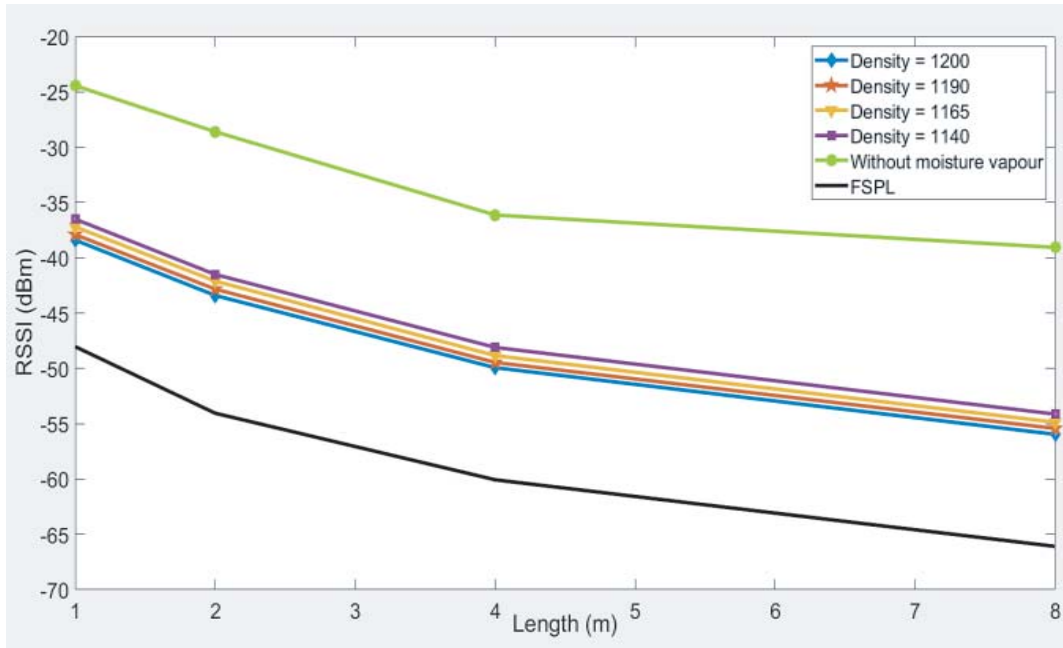
Figure 8. RSSI obtained through RT simulation considering moisture vapor density present in air flowing through the HVAC duct.
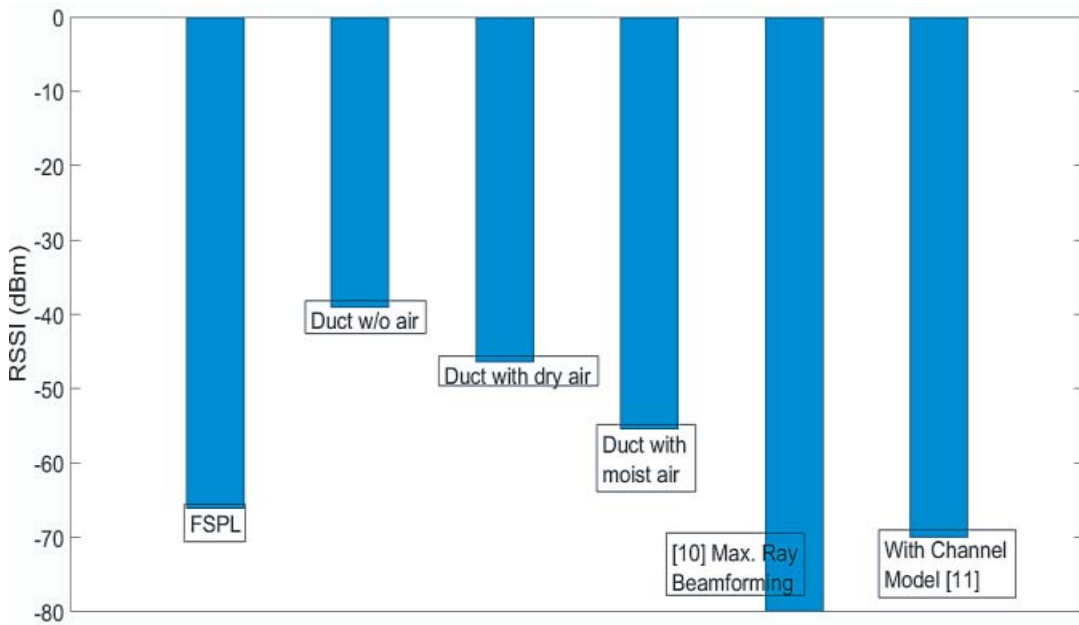
Figure 9. Comparison of RSSI obtained through 3D RT simulation, results from [9, 10] and FSPL.

ducts will not carry the air with moisture vapor. So, it suffices to say that HVAC duct outperforms the free space propagation in every situation.

In [9], the authors calculate the RSSI in the case of indoor communication where the transceiver is equipped to perform various beamforming techniques. The paper [9] considers indoor communication at 60 GHz, and the distance between the transmitter and receiver is 7 m. Similarly, the authors in [10] perform ray-tracing simulation considering the directional antennas for the indoor communication

environment at 60 GHz and record the values of the RSSI for the different receiver locations up to a distance of 8 m. The results from [9, 10] and the FSPL are compared to the RSSI values obtained through the RT simulation performed with the HVAC duct, without considering any air flowing, with air having a temperature of 30.15 K and with air having moisture vapor density of 1140 g/m^3 in Fig. 9. This figure shows that HVAC duct ray-tracing simulation results outperform all the previously recorded values of RSSI at 60 GHz for indoor communication and for similar separation distance and from FSPL by a margin of around 20 dBm. Table 1 gives an overview of the performance comparison of HVAC ducts with some of the other recent methodologies and studies done for millimeter wave communication. Further comparison results are presented in Table 1.

Table 1. Comparison of RSSI obtained through the use of HVAC duct and RSSI obtained using other techniques.

Ref.	Dist.	Frequency	Technique Used	Measurement	Ray-Tracing	RSSI (dBm)
[7]	2 m	70 GHz	Beam-forming	Custom mm-wave CS	Custom 3D	−91
[8]	5 m	60 GHz	Directional high gain antenna with max. ray beamforming	-	Ray launching RT	−80
[9]	6 m	58.5 GHz	Q-D channel with fading	Custom channel sounder	Clustering and diffuse scattering model	−70
[10]	4.5 m	60 GHz	Biconical omnidirectional antennas	Custom channel sounding system	-	−85
[11]	4 m	60 GHz	Polarimetric diffuse scattering channel model	Custom channel sounding system	-	−85
[12]	4 m	60 GHz	Ray path inference by beam pattern of phased array	SiBeam Phased array	Scenargie RT simulator	−50
[13]	5.4 m	60 GHz	Beam-forming	Custom mm-wave CS	-	−90
[14]	10 m	60 GHz	-	Hittite HMC6000LP711E	-	−100
[15]	6 m	60 GHz	Omnidirectional antenna SAGE 5836230230-15-S1		Custom 3D in MATLAB	−85
FSPL	8 m	60 GHz	-	-	-	−68
HVAC	8 m	60 GHz	Without air	Custom mm-wave CS	Custom 3D IM in MATLAB	−47
HVAC	8 m	60 GHz	Air at a temp. of 288.15 K	Custom mm-wave CS	Custom 3D IM in MATLAB	−47
HVAC	8 m	60 GHz	Air with moisture of density 1200 g/m^3	Custom mm-wave CS	Custom 3D IM in MATLAB	−57

5. CONCLUSION

A 3-dimensional (3D) ray-tracing tool to justify the use of HVAC ducts for the distribution of mm-wave signals was proposed. The 3D ray tracing tool is subjected to the condition of operation in mm-wave frequency band and for symmetrical structures, which lead to the reduction in the time and memory required to run the simulation. We incorporated the attenuation parameters due to the dry air and moisture vapor flowing through the HVAC duct. The results obtained from the ray-tracing were further utilized to calculate RSSI. With transmitter EIRP of 7 dBm, we obtain RSSI which varies between −24 dBm and −38 dBm for dry atmospheric pressure and temperature of 1013.25 hPa and 294.26 K, respectively, and duct lengths up to 8 m at 60 GHz. The results were compared with the experimental results, and we observe that the 3D ray tracing results closely match the experimental results, which further justifies the use of HVAC ducts for the distribution of mm-wave signals in an indoor environment. Future work will include extending the 3D ray tracing simulation for the HVAC ducts with different shapes and bends.

APPENDIX A.

In order to arrive at the general expression of the angle of incident, we consider a situation where three reflections have occurred. For a ray which undergoes three reflections, p_u can be divided into six parts as $p_u = p_{u1} + p_{u2} + p_{u3} + p_{u4} + p_{u5} + p_{u6}$ as shown in Fig. A1. The angle which the transmitted wave makes with the normal to the upper duct wall is represented as θ_{u3}.
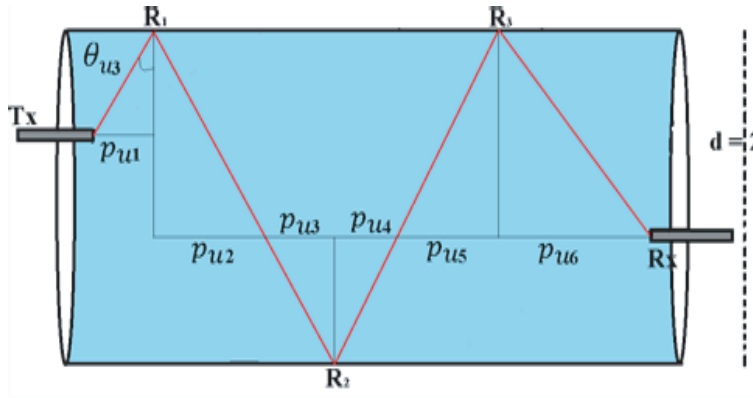
Figure A1. Ray tracing with three reflections inside the HVAC duct.

Therefore, the distances between the transmitter T_x, different reflection points and the receiver R_x, the tangent of the angle θ_{u3} can be represented as θ_{u3}.

Therefore, the distances between the transmitter T_x, different reflection points and the receiver R_x, the tangent of the angle θ_{u3} can be represented as

$$\tan(\theta_{u3}) = \frac{p_{u1}}{d - z_T} = \frac{p_{u2}}{d - z_R} = \frac{p_{u3}}{z_R} = \frac{p_{u4}}{z_R} = \frac{p_{u5}}{d - z_R} = \frac{p_{u6}}{d - z_R} = \frac{p_u}{d - z_T + 3d - z_R} \cong \frac{p_u}{4d - 2z} \quad (A1)$$

The last part of Eq. (A1) is calculated using $z_T \cong z_R$. Also, using the process described above, we can calculate the perpendicular distance between the reflection points and the projections for a ray that undergoes n odd or even number of reflections. For a ray that makes odd number of reflections, the total perpendicular distance will be equal to

$$(d - z_T) + n(d - z_R) + (n - 1) z_R \quad (A2)$$

Similarly, for a ray that makes even number of reflections, the total perpendicular distance will be equal to

$$(d - z_T) + (n - 1)(d - z_R) + n z_R \quad (A3)$$

Using Eqs. (A2), (A3), and assuming that $z_T \cong z_R$, we arrive at the denominator in Eq. (9).
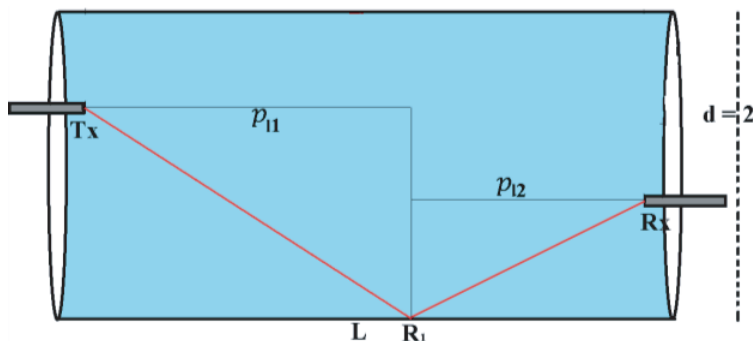
Figure A2. Ray tracing with one reflection inside the HVAC duct.

For the rays which are directed in the downward direction, we perform similar steps as that for the upward directed rays to arrive at Eq. (10). For a ray which has one reflection point R_1 on the lower duct wall (Fig. A2), $p_l = p_{l1} + p_{l2}$. The tangent of the angle which the ray makes with the lower duct wall is given in terms of p_l as

$$\tan(\theta_{l1}) = \frac{p_{l1}}{z_T} = \frac{p_{l2}}{z_R} = \frac{p_l}{z_T + z_R} \approx \frac{p_l}{2z_T} \tag{A4}$$

If a ray is reflected twice (Fig. A3), once from the lower wall R_1 and then from the upper wall R_2, then p_l can be divided into four parts as $p_l = p_{l1} + p_{l2} + p_{l3} + p_{l4}$. The angle which the transmitted wave makes with the normal to the lower duct wall is represented as θ_{l2}.
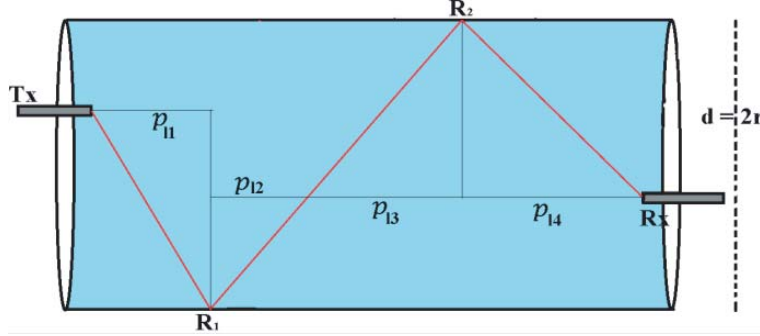
Figure A3. Ray tracing with two reflections inside the HVAC duct.

Therefore, the tangent of the angle θ_{l2} can be represented as

$$\tan(\theta_{l2}) = \frac{p_{l1}}{z_T} = \frac{p_{l4}}{d - z_R} = \frac{p_{l3}}{d - z_R} = \frac{p_{l2}}{z_R} = \frac{p_l}{z_T + 2(d - z_R) + z_R} \approx \frac{p_l}{2d} \tag{A5}$$

If a ray is reflected three times (Fig. A4), twice from the lower wall R_1 and R_3 and once from the upper wall R_2, then p_l can be divided into six parts as $p_l = p_{l1} + p_{l2} + p_{l3} + p_{l4} + p_{l5} + p_{l6}$. The angle which the transmitted wave makes with the normal to the lower duct wall is represented as θ_{l3}. Therefore, the tangent of the angle θ_{l3} can be represented as

$$\tan(\theta_{l3}) = \frac{p_{l1}}{z_T} = \frac{p_{l2}}{z_R} = \frac{p_{l3}}{d - z_R} = \frac{p_{l4}}{d - z_R} = \frac{p_{l5}}{z_R} = \frac{p_{l6}}{z_R}$$
$$= \frac{p_l}{z_T + 2(d - z_R) + 3z_R} = \frac{p_l}{2d + z_T + z_R} \approx \frac{p_l}{2d + 2z} \tag{A6}$$

The last part of Eq. (A6) is calculated using $z_T \cong z_R$. For a ray that makes odd number of reflections, the total perpendicular distance will be equal to

$$z_T + (n - 1)(d - z_R) + n z_R \tag{A7}$$
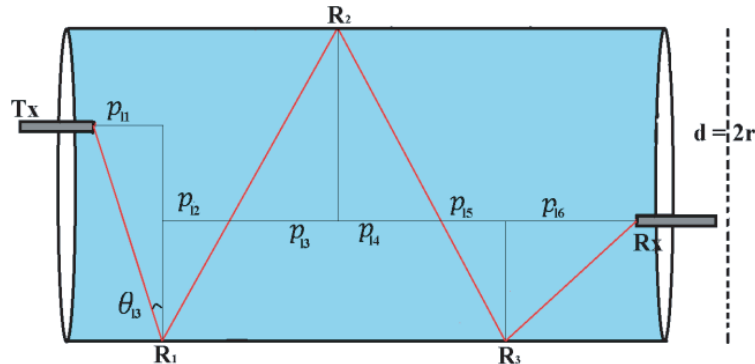
Figure A4. Ray tracing with three reflections inside the HVAC duct.

Similarly, for a ray that makes even number of reflections, the total perpendicular distance will be equal to

$$z_T + n\,(d - z_R) + (n - 1)\,z_R \tag{A8}$$

Using Eqs. (A7), (A8) and assuming $z_T \cong z_R$, we arrive at Eq. (10).

REFERENCES

1. Bangar, E. and K. Kiasaleh, "Experimental validation of the performance of heating, ventilation and air conditioning ducts as communication channel at 60 GHz," *2020 IEEE International Symposium on Local and Metropolitan Area Networks (LANMAN)*, 1–2, 2020.

2. Bangar, E., N. Taherkhani, and K. Kiasaleh, "Characterization of indoor heating, ventilation and air conditioning duct system as a communication channel at 60 GHz," *2020 IEEE Texas Symposium on Wireless and Microwave Circuits and Systems (WMCS)*, 1–7, 2020.

3. Yun, Z. and M. F. Iskander, Ray tracing for radio propagation modeling: Principles and applications," *IEEE Access*, Vol. 3, 1089–1100, 2015.

4. Holt, T., K. Pahlavan, and J. F. Lee, "A graphical indoor radio channel simulator using 2D ray tracing," *[1992 Proceedings] The Third IEEE International Symposium on Personal, Indoor and Mobile Radio Communications*, 411–416, 1992.

5. Liu, C. G., E. T. Zhang, Z. P. Wu, and B. Zhang, "Modelling radio wave propagation in tunnels with ray-tracing method," *2013 7th European Conference on Antennas and Propagation (EuCAP)*, 2317–2321, 2013.

6. Gündüzalp, E., G. Yildirim, and Y. Tatar, "Radio propagation prediction using SBR in a tunnel with narrow cross-section and obstacles," *2019 International Conference on Applied Automation and Industrial Diagnostics (ICAAID)*, 1–6, 2019.

7. Fuschini, F., M. Zoli, E. M. Vitucci, M. Barbiroli, and V. Degli-Esposti, "A study on millimeter-wave multiuser directional beamforming based on measurements and ray tracing simulations," *IEEE Transactions on Antennas and Propagation*, Vol. 67, No. 4, 2633–2644, April 2019.

8. Genc, Z., W. V. Thillo, A. Bourdoux, and E. Onur, "60 GHz PHY performance evaluation with 3D ray tracing under human shadowing," *IEEE Wireless Communications Letters*, Vol. 1, No. 2, 117–120, April 2012.

9. Kim, M., S. Kishimoto, S. Yamakawa, and K. Guan, "Millimeter-wave intra-cluster channel model for in-room access scenarios," *IEEE Access*, Vol. 8, 82042–82053, 2020.

10. Semkin, V., A. Karttunen, J. Järveläinen, S. Andreev, and Y. Koucheryavy, "Static and dynamic millimeter-wave channel measurements at 60 GHz in a conference room," *12th European Conference on Antennas and Propagation (EuCAP 2018)*, 1–5, 2018.

11. Freire, A. L., et al., "Polarimetric diffuse scattering channel measurements at 26 GHz and 60 GHz," *2018 IEEE 29th Annual International Symposium on Personal, Indoor and Mobile Radio Communications (PIMRC)*, 210–214, 2018.

12. Balakrishnan, S., et al., "60 GHz multipath propagation analysis and inference for an indoor scenario," *2020 IEEE 92nd Vehicular Technology Conference (VTC2020-Fall)*, 1–5, 2020.

13. Comiter, M., et al., "Millimeter-wave field experiments with many antenna configurations for indoor multipath environments," *2017 IEEE Globecom Workshops (GC Wkshps)*, 1–6, 2017.

14. Fernández, M., L. Zhang, S. L. Cotton, and D. Guerra, "Path loss measurements of user equipment to access point communications at 60 GHz," *2020 IEEE International Symposium on Broadband Multimedia Systems and Broadcasting (BMSB)*, 1–5, 2020.

15. Sheikh, M. U., K. Ruttik, R. Jäntti, and J. Hämäläinen, "Measurements and ray tracing simulations: Impact of different antenna positions on meeting room coverage at 60 GHz," *2020 European Conference on Networks and Communications (EuCNC)*, 63–67, 2020.

16. Chandra, K., R. V. Prasad, B. Quang, and I. G. M. M. Niemegeers, "CogCell: Cognitive interplay between 60 GHz picocells and 2.4/5 GHz hotspots in the 5G era," *IEEE Communications Magazine*, Vol. 53, No. 7, 118–125, July 2015.

17. Hajj, M. E., G. El Zein, G. Zaharia, H. Farhat, and S. Sadek, "Angular measurements and analysis of the indoor propagation channel at 60 GHz," *2019 International Conference on Wireless and Mobile Computing, Networking and Communications (WiMob)*, 121–126, 2019.

18. Kacou, M., V. Guillet, G. El Zein, and G. Zaharia, "Coverage and throughput analysis at 60 GHz for indoor WLAN with indirect paths," *2018 IEEE 29th Annual International Symposium on Personal, Indoor and Mobile Radio Communications (PIMRC)*, 1–5, 2018.

19. El Hajj, M., G. Zaharia, G. El Zein, H. Farhat, and S. Sadek, "Millimeter-wave propagation measurements at 60 GHz in indoor environments," *2019 International Symposium on Signals, Circuits and Systems (ISSCS)*, 1–4, 2019.

20. Wu, X., et al., "60-GHz millimeter-wave channel measurements and modeling for indoor office environments," *IEEE Transactions on Antennas and Propagation*, Vol. 65, No. 4, 1912–1924, April 2017.

21. Li, S., Y. Liu, L. Lin, D. Sun, S. Yang, and X. Sun, "Simulation and modeling of millimeter-wave channel at 60 GHz in indoor environment for 5G wireless communication system," *2018 IEEE International Conference on Computational Electromagnetics (ICCEM)*, 1–3, 2018.

22. Kimura, Y. and Y. Tsunemitsu, "Analysis of effective coverage area in 60 GHz-band millimeter wave wireless LAN for high speed railway passenger car and indoor room," *2019 International Symposium on Antennas and Propagation (ISAP)*, 1–3, 2019.

23. Sun, D., Y. Liu, and S. Li, "Simulation and analysis of 60 GHz millimeter-wave propagation characteristics in corridor environment," *2018 International Conference on Microwave and Millimeter Wave Technology (ICMMT)*, 1–3, 2018.

24. AlAbdullah, A. A., N. Ali, H. Obeidat, R. A. Abd-Alhmeed, and S. Jones, "Indoor millimetre-wave propagation channel simulations at 28, 39, 60 and 73 GHz for 5G wireless networks," *2017 Internet Technologies and Applications (ITA)*, 235–239, 2017.

25. Zhou, A., J. Huang, J. Sun, Q. Zhu, C. Wang, and Y. Yang, "60 GHz channel measurements and ray tracing modeling in an indoor environment," *2017 9th International Conference on Wireless Communications and Signal Processing (WCSP)*, 1–6, 2017.

26. Wang, M., Y. Liu, S. Li, and Z. Chen, "60 GHz millimeter-wave propagation characteristics in indoor environment," *2017 IEEE 9th International Conference on Communication Software and Networks (ICCSN)*, 749–752, 2017.

27. Sheng, Z., Y. Liu, Z. Chen, S. Li, and X. Zhang, "Study on the RMS and path loss of 60 GHz millimeter-wave in typical indoor environment," *2017 Sixth Asia-Pacific Conference on Antennas and Propagation (APCAP)*, 1–3, 2017.

28. Ruan, J. and Y. Zhang, "Simulation of 60 GHz millimeter-wave propagation characteristics based on SBR method in stairwell," *2019 International Applied Computational Electromagnetics Society Symposium — China (ACES)*, 1–2, 2019.

29. Rose, D. M., S. Rey, and T. Kürner, "Differential 3D ray-launching using arbitrary polygonal shapes in time-variant indoor scenarios," *2016 Global Symposium on Millimeter Waves (GSMM) & ESA Workshop on Millimetre-Wave Technology and Applications*, 1–4, 2016.

30. Kazemi, M. J., A. Abdipur, and A. Mohammadi, "Indoor propagation MIMO channel modeling in 60 GHz using SBR based 3D ray tracing technique," *2012 Second Conference on Millimeter-Wave and Terahertz Technologies (MMWaTT)*, 25–28, 2012.

31. Yue, G., D. Yu, H. Qiu, K. Guan, L. Yang, and Q. Lv, "Measurements and ray tracing simulations for non-line-of-sight millimeter-wave channels in a confined corridor environment," *IEEE Access*, Vol. 7, 85066–85081, 2019.

32. Horikoshi, S., M. Fuji, M. Itami, and K. Itoh, "A study on multipath propagation modeling in millimeter wave IVC," *The 5th International Symposium on Wireless Personal Multimedia Communications*, Vol. 1, 286–290, Honolulu, HI, USA, 2002.

33. Nikitin, P. V., D. D. Stancil, O. K. Tonguz, A. E. Xhafa, A. G. Cepni, and D. Brodtkorb, "RF propagation in an HVAC duct system: impulse response characteristics of the channel," *IEEE Antennas and Propagation Society International Symposium, (IEEE Cat. No.02CH37313)*, Vol. 2, 726–729, 2002.

34. Kermani, M. H. and M. Kamarei, "A ray-tracing method for predicting delay spread in tunnel environments," *2000 IEEE International Conference on Personal Wireless Communications. Conference Proceedings (Cat. No.00TH8488)*, 538–542, 2000.

35. Yang, C.-F., B.-C. Wu, and C.-J. Ko, "A ray-tracing method for modeling indoor wave propagation and penetration," *IEEE Transactions on Antennas and Propagation*, Vol. 46, No. 6, 907–919, June 1998.

36. Lee, S.-W. and G. Deschamps, "A uniform asymptotic theory of electromagnetic diffraction by a curved wedge," *IEEE Transactions on Antennas and Propagation*, Vol. 24, No. 1, 25–34, January 1976.

37. Dudley, D. G., M. Lienard, S. F. Mahmoud, and P. Degauque, "Wireless propagation in tunnels," *IEEE Antennas and Propagation Magazine*, Vol. 49, No. 2, 11–26, April 2007.

38. Balanis, C. A., *Advanced Engineering Electromagnetics*, 2nd Edition, Wiley, 2012.